

See discussions, stats, and author profiles for this publication at: <https://www.researchgate.net/publication/254863442>

# Spatial and Temporal Relationships among NDVI, Climate Factors, and Land Cover Changes in Northeast Asia from 1982 to 2009

Article in *GIScience & Remote Sensing* · July 2011

DOI: 10.2747/1548-1603.48.3.371

CITATIONS

34

READS

1,251

5 authors, including:



Yang Liu

Ocean University of China

59 PUBLICATIONS 376 CITATIONS

[SEE PROFILE](#)



Xiufeng Wang

Hokkaido University

144 PUBLICATIONS 1,407 CITATIONS

[SEE PROFILE](#)



Meng Guo

Northeast Normal University

48 PUBLICATIONS 815 CITATIONS

[SEE PROFILE](#)



Nobuhiro Matsuoka

Chiba University

38 PUBLICATIONS 293 CITATIONS

[SEE PROFILE](#)

Some of the authors of this publication are also working on these related projects:



Project

Using Greenhouse Gas Monitoring Satellite to Observe the Variation of Ecological Environment [View project](#)



Project

Natural Resource Management [View project](#)

# **Spatial and Temporal Relationships among NDVI, Climate Factors, and Land Cover Changes in Northeast Asia from 1982 to 2009**

**Yang Liu<sup>1</sup>, Xiufeng Wang, Meng Guo, and Hiroshi Tani**

*Graduate School of Agriculture, Hokkaido University,  
Sapporo, Japan, 060–8589*

**Nobuhiro Matsuoka**

*Faculty of Horticulture, Chiba University,  
Matsudo City, Chiba Prefecture, Japan 271-8510*

**Shinji Matsumura**

*Faculty of Agriculture, Kagawa University,  
Takamatsu City, Kagawa Prefecture, Japan, 760–8521*

---

**Abstract:** This study uses a multiple linear regression method to composite standard Normalized Difference Vegetation Index (NDVI) time series (1982–2009) consisting of three kinds of satellite NDVI data (AVHRR, SPOT, and MODIS). This dataset was combined with climate data and land cover maps to analyze growing season (June to September) NDVI trends in northeast Asia. In combination with climate zones, NDVI changes that are influenced by climate factors and land cover changes were also evaluated. This study revealed that the vegetation cover in the arid, western regions of northeast Asia is strongly influenced by precipitation, and with increasing precipitation, NDVI values become less influenced by precipitation. Spatial changes in the NDVI as influenced by temperature in this region are less obvious. Land cover dynamics also influence NDVI changes in different climate zones, especially for bare ground, cropland, and grassland. Future research should also incorporate higher-spatial-resolution data as well as other data types (such as greenhouse gas data) to further evaluate the mechanisms through which these factors interact.

---

## **INTRODUCTION**

Since the 2009 COP-15 Copenhagen Climate Conference, global climate and environmental variations have continued to capture the attention of national governments, researchers, and the public. Studies concerning variations of vegetation coverage on the earth's surface provide important data for understanding variations in the global environment (Fensholt et al., 2009). Research has shown that many factors cause variations in vegetation coverage, including long-term climate patterns, geographic or environmental changes, and human activities, such as industrialization and

---

<sup>1</sup>Corresponding author; email: yangliu315@hotmail.co.jp

agricultural development. Remote sensing data are highly effective for studying the relationship between vegetation and climate because they provide information at both temporal and spatial scales (Tucker et al., 2001; Gu et al., 2007). Currently existing earth observation satellites provide a variety of tools for observing vegetation on the earth's surface, and many researchers have analyzed their data (Tucker et al., 2005; Tarnacsky et al., 2008; Fensholt et al., 2009). Satellite remote sensing system-derived Normalized Difference Vegetation Index (NDVI) values are generally recognized to be good indicators of terrestrial vegetation productivity. Because NDVI has been widely used to estimate green biomass (Prince, 1991), many investigators use NDVI as the basis for their research and emphasize the relationships between NDVI and other factors.

A variety of research methods has been applied to NDVI data: (1) the statistical characteristics of NDVI data have been correlated with vegetative responses to climatic fluctuations (Davenport and Nicholson, 1993; Anyamba and Eastman, 1996; Richard and Poccard, 1998; Wang et al., 2003); (2) the relationships between climate data and other factors, such as the NDVI during the growing season, the Leaf Area Index (LAI), the Net Primary Productivity (NPP), soil moisture, the index of the earth's surface, and land cover, have been evaluated through correlation or regression analysis (Tieszen et al., 1997; Gao and Dennis, 2001; Yu et al., 2003; Gu et al., 2007); and (3) NDVI and meteorological time series have been analyzed (Fensholt et al., 2006; Heumann et al., 2007; Verbesselt et al., 2010). The results of these analyses have indicated that NDVI has obvious relationships with primary climatic factors (precipitation and temperature); however, these relationships are specific to particular regions and vary significantly among different regions.

Northeast Asia includes six countries: the Russian Federation (primarily the Russian Far East), Mongolia, the People's Republic of China (eastern part of China), the Democratic People's Republic of Korea (DPRK), the Republic of Korea (ROK), and Japan. As is evident from this list, northeast Asia has a great diversity of political and economic systems as well as various levels of economic development. Since 2000, the rate of economic growth in this region has been exceptional, especially in Japan, the ROK, and China. This growth has reflected the rapidly expanding technological strength of these countries. Rapid development has caused corresponding changes in the natural environment and has contributed to many environmental and natural resource problems. During rapid industrialization and population growth, vegetation is vulnerable to direct anthropogenic effects (such as land development) and indirect anthropogenic effects (such as climate change, acid rain, and air pollution).

This study is intended to achieve three primary goals. First, because satellite data encompass data from a variety of sensors and time periods, we explore the creation of continuous long-term NDVI data based on three kinds of widely used NDVI satellite data to more effectively analyze environmental vegetation changes: Advanced Very High Resolution Radiometer (AVHRR) Global Inventory Modeling and Mapping Studies (GIMMS) NDVI data, SPOT VGT NDVI data, and Terra MODerate resolution Imaging Spectroradiometer (MODIS) NDVI data. Second, we analyze the relationships between NDVI, climate factors, and land cover classifications in combination with climate zones to establish their interactions and to understand the mechanisms that underlie their variation. Finally, we provide fundamental data to support Japan's Greenhouse Gases Observing Satellite "IBUKI" (GOSAT) project-related research,

which implements the world's first satellite for observing concentrations of carbon dioxide and methane from space. The GOSAT project will facilitate future studies of the relationship between greenhouse gas emissions and variations in environmental vegetation, in addition to the influence of human activities on the ecosystem.

## STUDY AREA AND DATA USED

### Study Area

The study area encompasses the northeastern part of the Asian continent, including approximately 5,125,000 km<sup>2</sup> of land extending from 30° N to 55° N Latitude and from 110° E to 150° E Longitude. Most of northeastern Asia is mountainous. Large swaths of the area are forested, including far eastern Russia, the mountainous region of northeastern China, the Korean Peninsula, and most of Japan. Cropland covers the northeastern China plains and most of southeastern China, and grassland covers Mongolia, the southern part of far eastern Russia, Inner Mongolia, and part of northeastern China. On the whole, vegetative cover gradually increases from west to east.

In terms of climate, northeast Asia spans a wide range of latitudes and includes both vast mountainous regions and plateaus. Each region experiences different land and ocean influences, and extreme variations in climate factors create a highly complex regional climate system. Summer is megathermal and rainy with predominant southerly winds, whereas winter is cold and dry with predominant northerly winds. With the exception of the mountainous region east of the Sea of Japan and the plains area along the Sea of Japan, which are rainy, northeastern Asia is rainless during the winter.

### NDVI Data

**AVHRR GIMMS 15-Day Composite NDVI Data.** The GIMMS dataset is an NDVI product that is available for the 25-year period from 1981 to 2006. This dataset is derived from imagery that was obtained from the AVHRR instruments onboard NOAA satellite series 7, 9, 11, 14, 16, and 17. The NOAA AVHRR Global Area Coverage (GAC) 1B data (Goward et al., 1993), which are the inputs for the GIMMS land data processing, are derived at a resolution of 4 × 4 km from the onboard averaging and sampling of 1.1 km full-resolution Local Area Coverage (LAC) data (Townshend, 1994). In every third scan line, the first four of five pixels are averaged to generate a nadir cell of 1.1 km × 4 km in size with 2.2 km gaps across the scan lines (Kidwell, 1990). Each GAC pixel is binned into one of the 8 km pixels of the output product based on a forward, nearest-neighbor mapping method, which selects the GAC pixel with the highest NDVI value (James and Kalluri, 1994).

This NDVI dataset is corrected for calibration, viewing geometry, volcanic aerosols, and other effects that are not related to vegetation changes (Tucker et al., 2004). The GIMMS dataset is composited at 15 day intervals. The 15a composite is the maximum value composite from the first 15 days of the month, whereas the second composite (15b) includes day 16 through the end of the month. This dataset was obtained from the Global Land Cover Facility ([www.landcover.org](http://www.landcover.org)).

**SPOT VGT 10-Day Composite NDVI Data.** The sensor design of the SPOT satellites (SPOT-4 and SPOT-5) enhances the AVHRR scanning array in terms of its spatial resolution distortion at off-nadir angles up to approximately 50° (SPOT Vegetation User's Guide, 2008). Furthermore, the SPOT VGT instruments offer advantages over the AVHRR sensors, including better navigation and improved radiometric sensitivity (Gobron et al., 2000). The 10-day synthesis product (S10) has a full  $1 \times 1$  km resolution derived from P products through maximum-value composite (MVC) NDVI syntheses (Holben, 1986). The S10 product has a cloud quality flag that is based on the threshold of the top of atmosphere (TOA) reflectance in each of the four bands, which are compared to reference reflectance maps for each band (Kempeneers et al., 2000; SPOT Vegetation User's Guide, 2008).

This dataset is composed of VEGETATION data from the SPOT-4 platform (launched in March 1998) and the SPOT-5 platform (launched in May 2002). The S10 data through January 2003 are available at <http://free.vgt.vito.be/origin> from SPOT-4 (VGT1 sensor), and after that time, the results are from SPOT-5 (VGT2 sensor). The spectral response functions (SRF) of the SPOT-4 and SPOT-5 bands are not identical and therefore can induce reflectance variations.

**Terra MODIS 16-Day Composite NDVI Data.** The 16-day composites of the Terra MODIS vegetation indices (MOD13 series) are designed to extend the 20-year NOAA dataset of the AVHRR-derived NDVI time series (Huete et al., 2002). MODIS NDVI data contain atmospherically corrected bidirectional surface reflectance masked for water, clouds, and cloud shadows. Version 5 MODIS/Terra NDVI products of the Global MOD13C1 data, which are obtained from <https://lpdaac.usgs.gov/lpdAAC/products/>, are cloud-free spatial composites of the gridded 16-day 1 km MOD13A2 data and are provided as a level-3 product projected on a  $0.05 \times 0.05$  degree ( $5,600 \times 5,600$  m) geographic Climate Modeling Grid (CMG). Cloud-free global coverage is achieved by replacing clouds with the historical MODIS time series climatology record.

## Land Cover Data

Given that the present study uses data from 1982 to 2009, simple land cover maps cannot reflect the region's land classification changes over a 28-year contiguous time period. Therefore, in this study, we selected two different periods of land cover data for analysis.

**AVHRR Global Land Cover (GLC) Data.** AVHRR GLC data were generated by the Department of Geography at the University of Maryland in 1998. Imagery that was acquired from the AVHRR satellites between 1981 and 1994 were analyzed to distinguish 14 land cover classes (Hansen et al., 1998). Additionally,  $1 \times 1$  km pixel resolution data were obtained from the Global Land Cover Facility and used in this study.

**European Space Agency Global Land Cover (ESA GLC) Data.** The ESA global land cover map was generated from 19 months of full spatial resolution Medium Resolution Imaging Spectrometer (MERIS)/ENVISAT data that were acquired during the period from May 2005 to April 2006. This map was produced as part of the GLOBCOVER project of the ESA by POSTEL/Medias-France, which was the primary contractor. The global land cover map has a spatial resolution of  $300 \times 300$  m and discriminates among the land surfaces of 22 representative continental ecosystems.

With the permission of the ESA, the data are publicly available through the POSTEL Service Centre (<http://www.esa.int/due/ionia/globcover>).

### Climate Data

**Global Precipitation Data.** The CPC Merged Analysis of Precipitation (CMAP) produces pentad and monthly analyses of global precipitation in which observations from rain gauges are merged with precipitation estimates from several satellite-based algorithms (Xie and Arkin, 1997). The analyses are based on a  $2.5 \times 2.5$  degree latitude-longitude grid and extend back to 1979. Monthly CMAP data are available from the CPC ftp server (<ftp://ftp.cpc.ncep.noaa.gov/precip/cmap>).

**Global Temperature Anomaly Data.** CRUTEM3 is a gridded dataset of global historical land surface temperature anomalies (Brohan et al., 2006). Data are available for each month since January 1850 on a  $5 \times 5$  degree latitude-longitude grid. The dataset is a collaborative product of the Met Office Hadley Centre and the Climatic Research Unit (CRU) at the University of East Anglia. The CRUTEM3v dataset, which has been variance adjusted, was used in this study. The CRUTEM3v datasets are available at the CRU website (<http://www.cru.uea.ac.uk/cru/data/temperature/>).

## METHODS

### NDVI Data Processing

All NDVI data were calculated as seasonal averages covering the growing season (June to September) to reduce the effects of considerable variations in latitude and altitude, incomplete information on the biophysical processes of vegetation, and different periods of vegetation growth (Chen et al., 2000). Data included AVHRR GIMMS NDVI data (1982–2009), SPOT VGT NDVI data (2003–2009), and Terra MODIS NDVI data (2003–2009). As mentioned above, the three datasets were derived from maximum NDVI images to minimize the effects of cloud contamination, scanning angle variability, sun angle, aerosols, and water vapor. To directly compare these data, we resampled the Terra MODIS  $5600 \times 5600$  m data and the SPOT VGT  $1 \times 1$  km NDVI data by spatial averaging to match the  $8 \times 8$  km AVHRR GIMMS resolution before calculating the NDVI.

### Compilation of Standard NDVI Curves

A standard NDVI variation curve was constructed for time series NDVI data based on the GIMMS data from 1982 to 2009 by interpolating the missing period (2007–2009) utilizing SPOT VGT and MODIS NDVI data. Because the SPOT data sensor changed in 2003, data from 2003 to 2006 were used. The algorithm to predict the GIMMS NDVI is based on a multiple linear regression analysis using a stepwise method. The GIMMS NDVI value at each pixel is expressed as a function of the SPOT VGT and MODIS NDVI value. Multiple linear regression models at a 95% significance level were adopted.

**Table 1.** Land Cover Classification Scheme

Land cover class	Description
Cropland	Post-flooding or irrigated croplands, and rain-fed cropland, livestock
Forest	Deciduous forest, evergreen forest, mixed forest, orchards, woodland
Grassland	Grass, shrubland, savannas or lichens, sparse, meadow
Bare	Beaches, exposed rock, and disturbed land
Urban	Artificial surfaces and associated areas
Water	Sea, streams, and waterways, lakes, reservoirs, bays, and estuaries

### Climate Data Processing

Global monthly precipitation data were compiled on a  $2.5 \times 2.5$  degree latitude-longitude grid for the 27-year period from 1982 to 2008. Data from 2009 were incomplete. Monthly “rain1” values, which include a numerical model in the form of a  $2.5 \times 2.5$  degree grid, were combined with annual data, interpolated into raster maps via the Kriging method (Jiang et al., 2008) using Surfer software, and then resampled to match the spatial resolution of the seasonal average NDVI data. The global surface monthly temperature anomalies dataset, CRUTEM3v, was processed by the same method as precipitation data from 1982 to 2008.

Based on annual temperature anomaly variance means from 1982 to the present (Fig. 1A), the temperature of the entire region has been gradually increasing. Areas near oceans have been relatively consistent. Precipitation values for the last 28 years illustrate major regional differences in the precipitation distribution and present a digressive trend from the humid east to the dry west (Fig. 1B). Southeastern China, the Korean peninsula, the islands of Japan, and the southern coastal area of far eastern Russia are monsoonal regions that are associated with summer rain, wherein the annual precipitation is approximately 800 to 1200 mm. Precipitation in continental northeastern Asia decreases from the east (800 mm) to the west (400 mm) as a function of distance from the ocean. The central region of Mongolia is effectively rainless, with an annual rainfall in most areas of less than 150–200 mm.

### Land Cover Data Processing

The land cover maps were reclassified into six classes (forest, grassland, cropland, urban, bare, and water) based on the land cover and land use classification system of the AVHRR GLC and ESA GLC (Table 1). All of the maps were also resampled to the same spatial resolution as the seasonal average NDVI data (Fig. 2).

### NDVI and Land Cover Change Detection

Temporal trends in the seasonal average NDVI data (1982–2009) were analyzed using a simple linear regression model in which time was the independent variable and the NDVI was the dependent variable (Fensholt et al., 2009). The trends were analyzed at a 95% confidence level using the standard *t*-test. For each pixel, the slopes of the linear regression and *r* values were extracted.

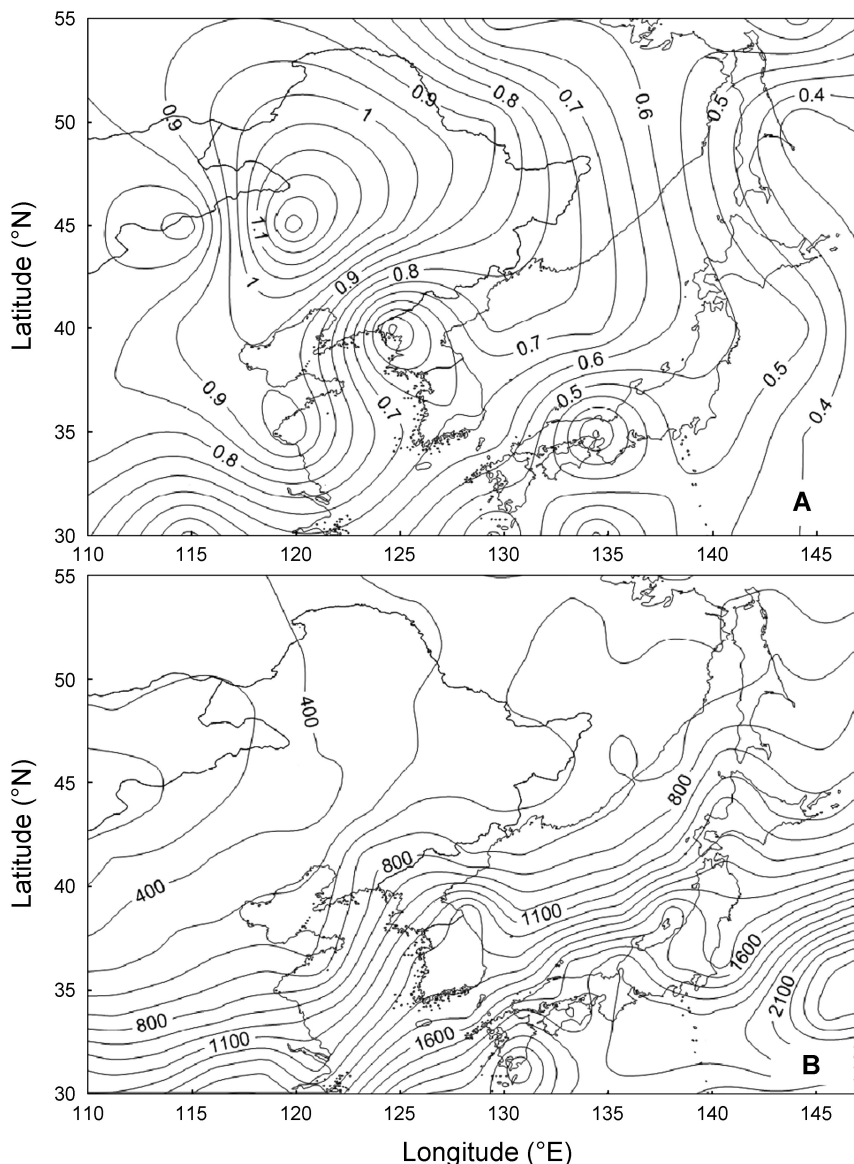


**Fig. 1.** A. Mean annual land surface temperature anomalies ( $^{\circ}\text{C}$ ), 1982–2008, derived from CRUTEM3v data. B. Annual precipitation (mm), 1982–2008, derived from CMAP data in northeast Asia.

A post-classification comparison change detection algorithm was used to determine changes in land cover in two datasets, the AVHRR GLC and the ESA GLC. The post-classification approach provides “from-to” change information and the kind of landscape transformations that have occurred can be easily calculated and mapped (Yuan et al., 2005).

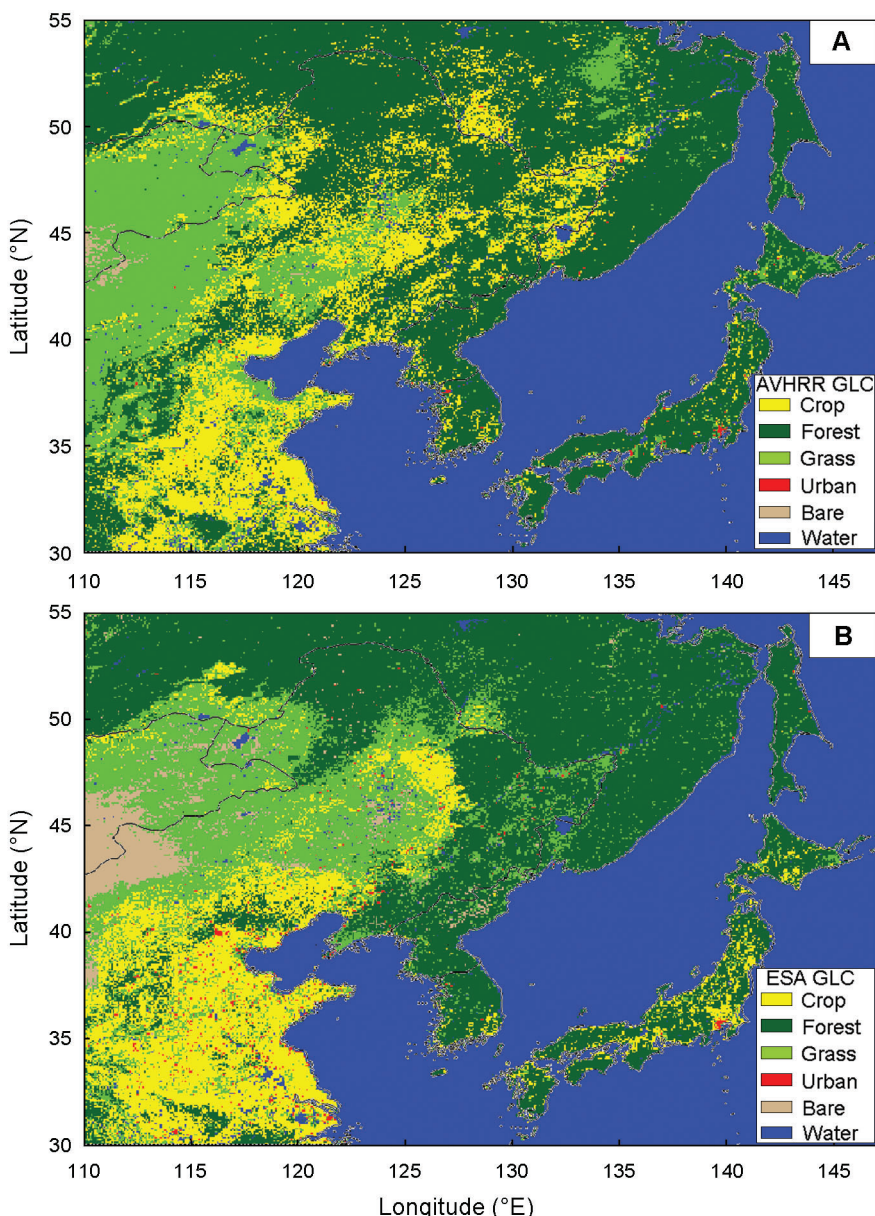


**Fig. 2.** Land cover map of northeast Asia derived from AVHRR GLC data (A) and ESA GLC data (B).

#### Analysis of Correlation between NDVI and Climatic Factor Variables

To analyze the relationships between changes in the NDVI and climatic factors, partial and multiple correlation coefficients were selected to reflect those relationships. Two indicators were analyzed, as described below.

**Partial Correlation Coefficients.** Partial correlation coefficients that were used in this study can be formulated as follows:

$$r_{xy} = \frac{\sum_{i=1}^n (x_i - \bar{x})(y_i - \bar{y})}{\sqrt{\sum_{i=0}^n (x_i - \bar{x})^2 \times \sum_{i=0}^n (y_i - \bar{y})^2}} \quad (1)$$

where  $x_i$  is the seasonal NDVI value,  $\bar{x}$  is the mean NDVI value in all years,  $y_i$  represents seasonal climatic factors (temperature or precipitation),  $\bar{y}$  is the mean value of temperature or precipitation in all years,  $n$  is the number of samples, and  $r_{xy}$  is the correlation coefficient between the NDVI and the climatic factors (temperature or precipitation).

$$r_{xy-z} = \frac{r_{xy} - r_{xz} \times r_{yz}}{\sqrt{(1 - r_{xz}^2)(1 - r_{yz}^2)}} \quad (2)$$

where  $r_{xy}$ ,  $r_{xz}$ , and  $r_{yz}$  are correlation coefficients between the NDVI and temperature, the NDVI and precipitation, and temperature and precipitation, respectively, and  $r_{xy-z}$  is the partial correlation coefficient between two factors based on a third factor. The  $t$ -test method was adopted to test the partial correlation coefficients. The  $t$ -test equation was formulated as follows:

$$t = \frac{r_{xy-z}}{\sqrt{1 - r_{xy-z}^2}} \sqrt{n - m - 1} \quad (3)$$

where  $r_{xy-z}$  is the partial correlation coefficient between two factors based on a third factor,  $n$  is the number of samples,  $m$  is an independent variable, and  $t$  is the testing value.

**Multiple Correlation Coefficients.** The multiple correlation coefficients used in this study can be formulated as follows:

$$r_{x-yz} = \sqrt{1 - (1 - r_{xy}^2)(1 - r_{xz-y}^2)} \quad (4)$$

where  $r_{xy}$  is the correlation coefficient between the NDVI and climatic factors (temperature or precipitation),  $r_{xz-y}$  is the partial correlation coefficient between two factors based on a third factor, and  $r_{x-yz}$  is the multiple correlation coefficient between the NDVI and the two aforementioned climatic factors.

The  $f$ -test method was adopted to test the multiple correlation coefficients. The  $f$ -test equation was formulated as follows:

$$f = \frac{r_{x-yz}}{1 - r_{x-yz}^2} \times \frac{n - k - 1}{k}, \quad (5)$$

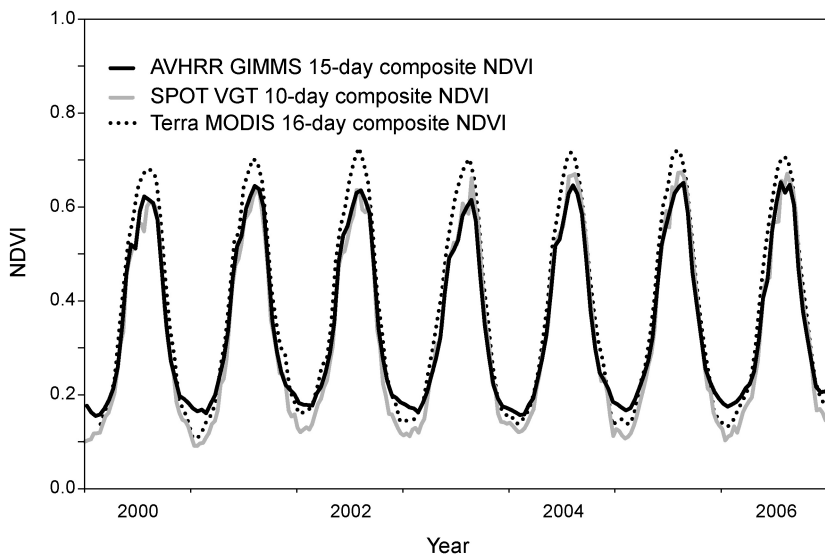


**Fig. 3.** Time series of AVHRR GIMMS, SPOT-VGT, and Terra MODIS NDVI from northeast Asia, 2000–2006.

where  $r_{x-yz}$  are multiple correlation coefficients between NDVI and the two climatic factors,  $n$  is the number of samples,  $k$  is an independent variable, and  $f$  is the testing value.

## RESULTS AND DISCUSSION

### Analysis of Spatial Trends in Standard NDVI

Because GIMMS, SPOT VGT, and Terra MODIS NDVI data are derived from different sensors and wave ranges (Fig. 3), it was necessary to evaluate their consistency. The compiled results indicate that the average NDVI values for the entire study area were lowest at the end of January and beginning of February and highest at the end of July and beginning of August. In comparison, the MODIS maximum was relatively high (approximately 0.70), the GIMMS maximum was relatively low (approximately 0.62), the SPOT minimum was relatively low (approximately 0.12), and the GIMMS minimum was relatively high (approximately 0.18). The overall extent of variation was lowest for the GIMMS data, which is consistent with the conclusions of Fensholt (2009). Therefore, using SPOT VGT and MODIS NDVI data as two parameters in the multiple linear regression method employed in this study, GIMMS NDVI values can be more easily predicted.

Thus, continuous long-term NDVI data based on GIMMS data were predicted by utilizing the SPOT VGT and MODIS NDVI data. The results are shown in Eq. (6). The adjusted multiple correlation is 0.74, and GIMMS NDVI from 2007 to 2009 can be predicted.

$$\text{GIMMS} = 0.216 \times (\text{MODIS}) + 0.565 \times (\text{SPOT}) + 0.097 . \quad (6)$$

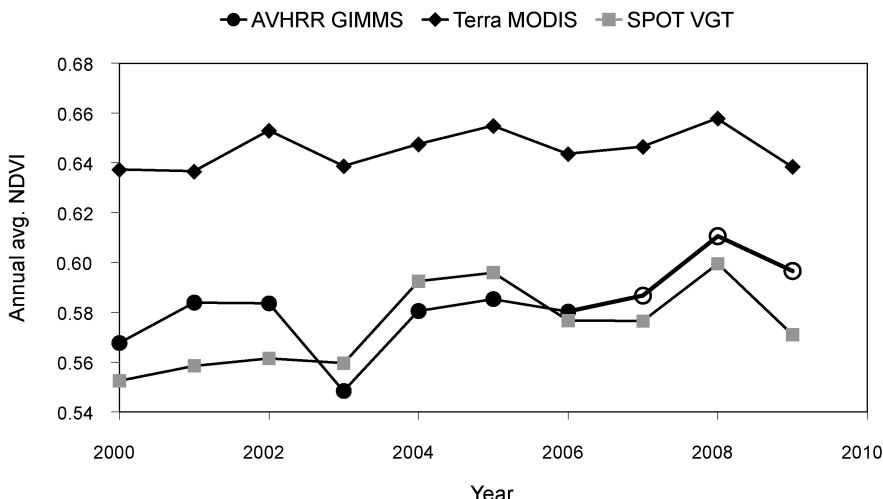


**Fig. 4.** Seasonal average of AVHRR GIMMS, SPOT-VGT, and Terra MODIS NDVI from northeast Asia, 2000–2009. GIMMS NDVI data, which are marked by the open circles, are calculated by a multiple linear regression method.

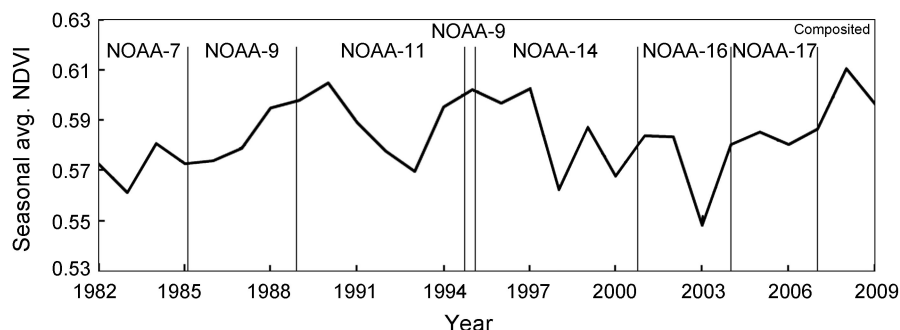


**Fig. 5.** Integrated seasonal average of standard NDVI variation in northeast Asia, 1982–2009 (thick line), and instrument change times for the GIMMS dataset (thin line).

The GIMMS NDVI data trends were observed to agree well with those of the two other kinds of data (Fig. 4). The calculated integrated seasonal average NDVI variation curve depicted in Figure 5 demonstrates that NDVI variation was related to the orbital drifts and discontinuities of the platforms. In Figure 5, we can observe that the changes in the calculated integrated seasonal average NDVI variation curve were not appreciably impacted by changes in the satellite platforms.

#### Analysis of the Relationships between the NDVI and Land Cover

Figure 6 summarizes 28 years of temporal trends based on a linear regression trend analysis of slope values derived from the standard NDVI time series. This method is a

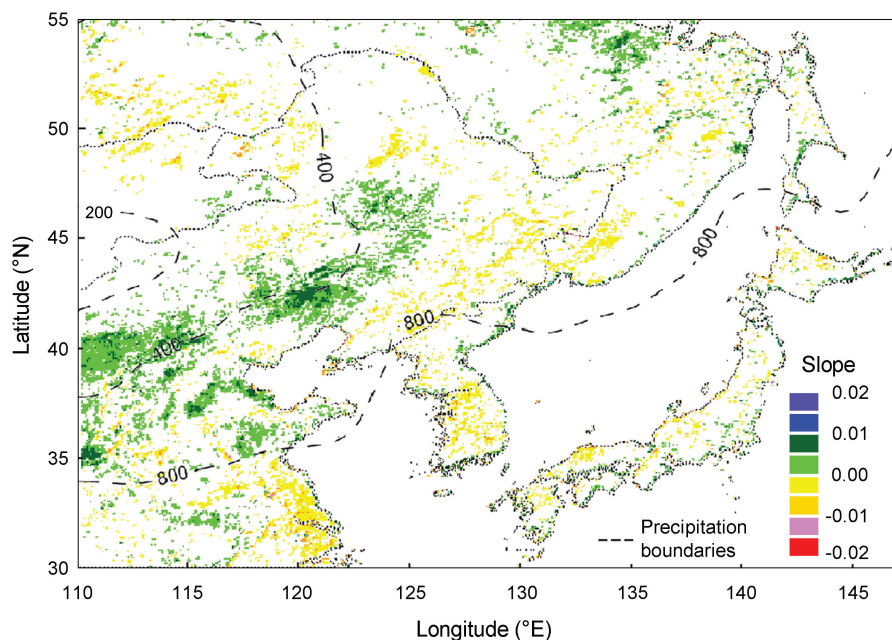


**Fig. 6.** Regression coefficient (slope) values for pixels ( $p < 0.05$ ) from linear regression trend analysis of standard NDVI, 1982–2009.

simple way to identify and analyze long-term trends in the NDVI. The pixel regression slopes, wherein the  $r$  value for the NDVI changes from 1982 to 2009, were greater than 0.37 ( $t$ -test  $p < 0.05$ ). Most of the slope values were in the range of  $-0.01$  to  $0.01$ , and the average regional slope was  $0.005$ , which indicates that the NDVI results exhibit a slightly increasing trend. Throughout the distribution of NDVI changes, the NDVI values depicted an obvious area increase of  $8.5\%$  for the entire land area that was associated with forest and grass cover, primarily in the middle region of northern China and the middle and lower reaches of the Yellow River of China. The NDVI values exhibited a clear area decrease of  $5.9\%$  for the entire land area in regions where there was mainly forest and cropland, primarily on the east coast of China and the Korean Peninsula.

Because different land cover maps are derived when using different classification methods from different satellite observation systems and do not consider differences among land classification methods, seasonal NDVI changes that are associated with different vegetation types were analyzed for two land cover maps. The results are shown in Figure 7. In general, the NDVI values for four major land classifications exhibited slightly increasing tendencies. The NDVI values for farmland and grassland were less variable (Figs. 7C and 7D), whereas NDVI changes for forest were larger. The forest NDVI values exhibited minima in 1982, 1993, 1998, and 2003 and peaks in 1989, 1995, 2001, and 2008, which indicates that cyclical changes occurred over periods of 2–5 years (Fig. 7B). From 2000 onward, the range of changes for bare ground increased (Fig. 7A).

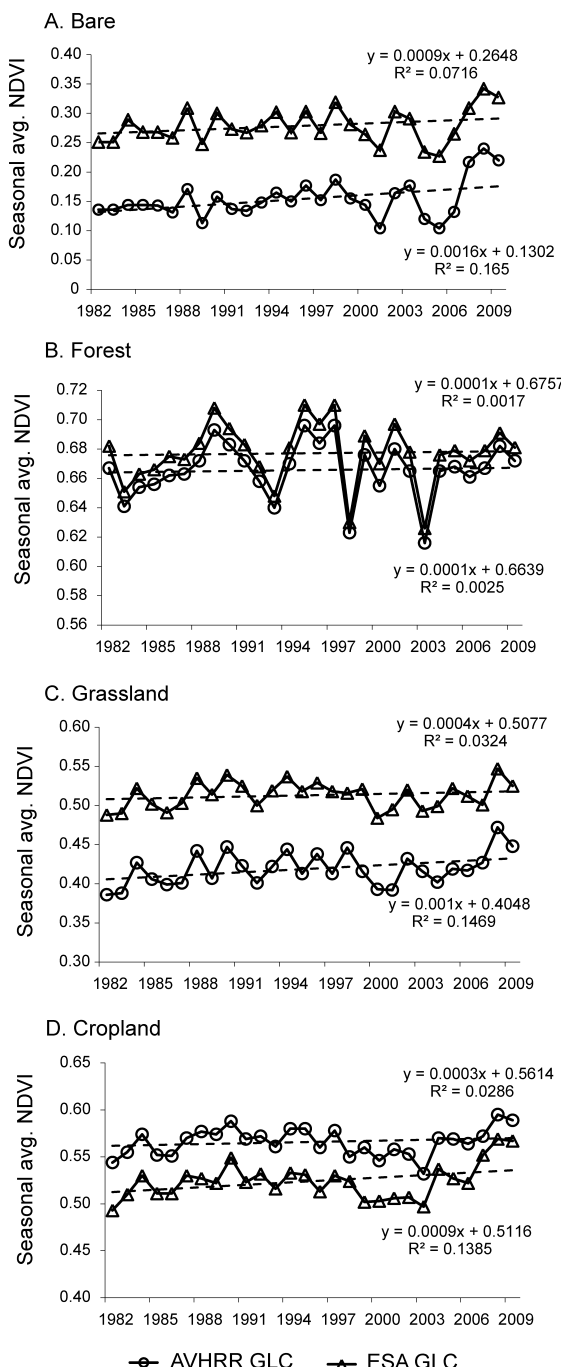


**Fig. 7.** Seasonal average NDVI change at different land cover classifications in AVHRR GLC and ESA GLC data, 1982–2009. A. Bare. B. Forest. C. Grassland. D. Cropland.

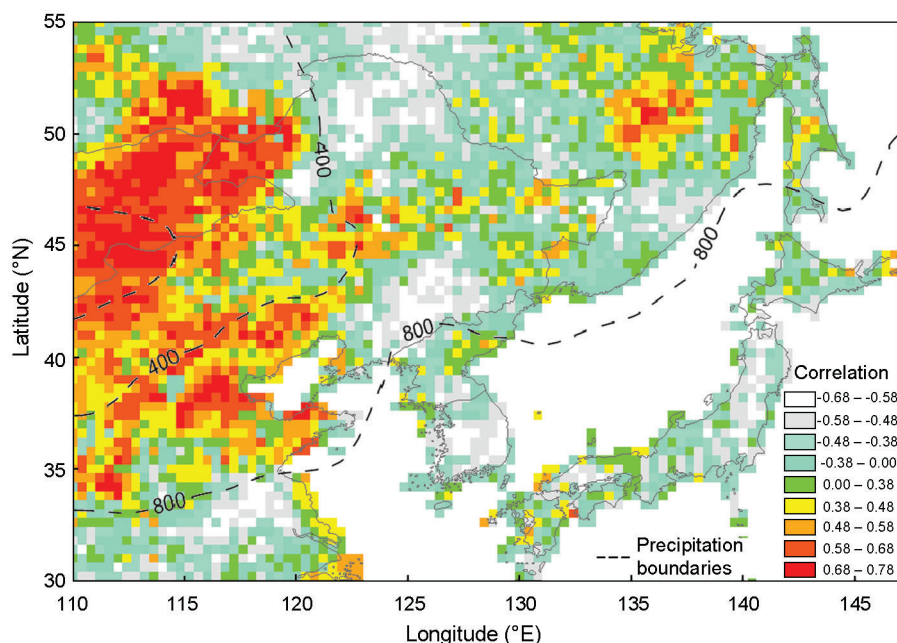
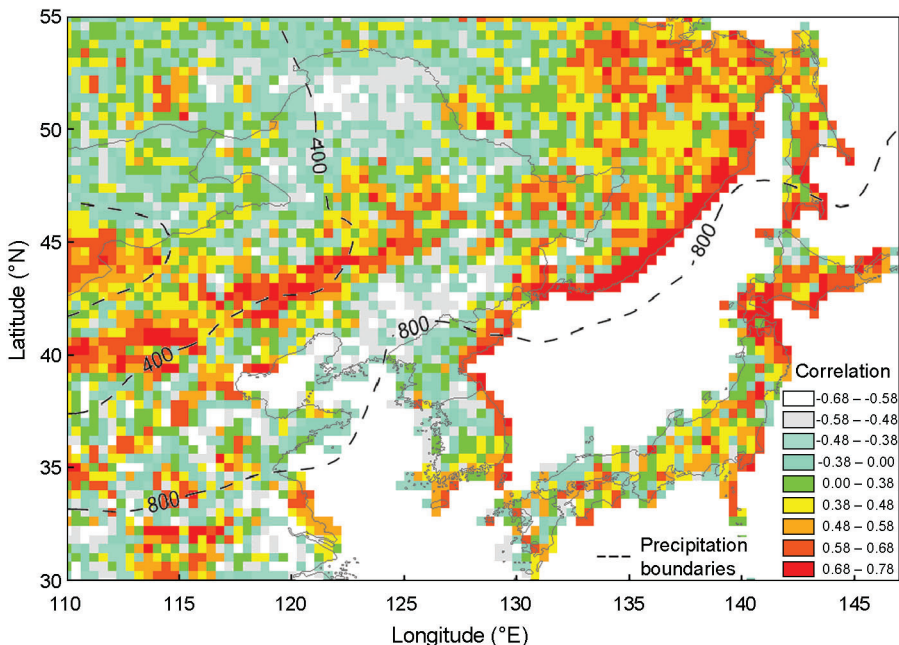


**Fig. 8.** Map of partial correlation coefficient between seasonal standard NDVI and precipitation based on temperature, 1982–2009.

A comparison of two different land cover types indicated that the changes in the NDVI values for the two land classifications were consistent, and this was especially evident in the small differences in the NDVI values for the forest classifications of the two datasets. With regard to bare ground and grassland, the NDVI values from ESA data were approximately 0.10 higher than the NDVI values that were derived from AVHRR data. For the classification of farmland, NDVI values that were obtained from ESA data were approximately 0.05 lower than those from AVHRR data. There are two possible explanations for this result. One involves system-based errors that are caused by differences in land classification maps that are derived from different satellite observation systems with different band wavelengths and spatial resolutions. The other reason involves changes in land cover classification for different periods. We can ignore the aforementioned system-based errors because we used data with a uniform spatial resolution and applied reclassification techniques. Thus, we find that in the study region NDVI changes are affected by changes in land cover and are particularly influenced by bare ground, cropland, and grassland.

### The Correlation between NDVI and Climate Variation

Seasonal average data from 1982 to 2008 (the NDVI, precipitation, and temperature) were used to compute the partial and multiple correlation coefficients at the pixel scale for the entire macroregion of northeast Asia. Statistical significance tests were based on the *t*-test (at a significance level of 0.05) and *f*-test (at a significance level of 0.05).



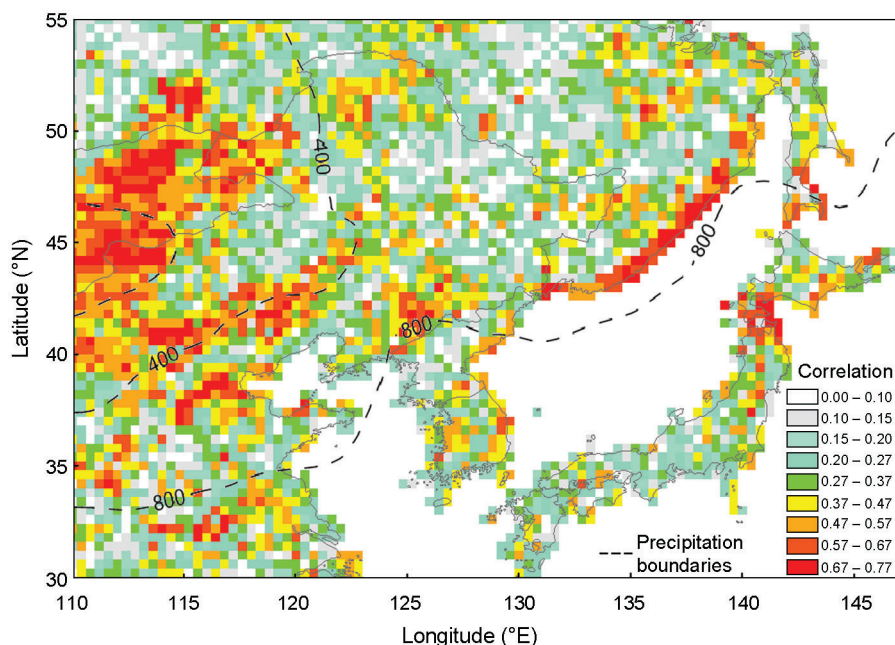
**Fig. 9.** Map of partial correlation coefficient between seasonal standard NDVI and temperature based on precipitation, 1982–2009.

Figure 8 is a map of the partial correlation coefficients between the seasonal average NDVI and the precipitation based on temperature. When the statistical significance level is 0.05, the partial correlation coefficients must be greater than 0.38. This map depicts the area where the strongest correlation between the NDVI and precipitation existed, covering 13.2% of the total land area, primarily in eastern Mongolia and along the middle and lower reaches of the Yellow River of China; however, for most of the area, the statistical relationship between the NDVI and precipitation was not significant.

Figure 9 is a map of the partial correlation coefficients between the seasonal average NDVI and temperature based on precipitation. The yellow and red areas correspond to regions where the partial correlation coefficients between NDVI and temperature were greater than 0.38. These yellow and red areas are distributed among scattered regions and are also found on the east coastal area of the continent that faces the Sea of Japan. These areas constitute only 12.4% of the entire land area.

Figure 10 is a map of the multiple correlation coefficients between the seasonal average NDVI and the two aforementioned climate factors. Multiple correlation coefficients of greater than 0.47 were found over 39.5% of the entire land area, particularly in the Inner Mongolia region of China and in Mongolia.

The results obtained describe nonuniform variability in the distribution of the joint driving action of temperature and precipitation on the NDVI. Therefore, to better analyze the correlations among the three factors in this region, the research area was divided into four climate zones, and climate types were assessed according to annual



**Fig. 10.** Map of multiple correlation coefficients between seasonal standard NDVI and two climate factors (precipitation, temperature), 1982–2009.

**Table 2.** Analysis of the Relationship between NDVI and Climate Factors for Different Climatic Zones from 1982 to 2008

	I	II	III	IV	Total
Annual precipitation (mm)	<200	200–400	400–800	>800	
Climate zones	Arid	Semi-arid	Subhumid	Humid	
Mean seasonal standard NDVI (Jun.–Sep.)	0.23	0.50	0.62	0.52	0.56
$r_{NDVI, Precip.-Temp.}^a$	0.55	0.22	-0.01	-0.14	0.02
$r_{NDVI, Temp.-Precip.}^b$	0.05	0.05	0.09	0.06	0.08
$r_{NDVI-Temp.-Precip.}^c$	0.59	0.38	0.33	0.32	0.34

<sup>a</sup> $r_{NDVI, Precip.-Temp.}$  is the partial correlation coefficient between standard NDVI and precipitation based on temperature.

<sup>b</sup> $r_{NDVI, Temp.-Precip.}$  is the partial correlation coefficient between standard NDVI and temperature based on precipitation.

<sup>c</sup> $r_{NDVI-Temp.-Precip.}$  is the multiple correlation coefficient between standard NDVI and precipitation, temperature.

precipitation (Wu et al., 2003). Table 2 presents the interactions between the NDVI and the climate factors for different climatic zones from 1982 to 2008.

The arid climate zone (I) is primarily located in part of southeastern Mongolia and receives less than 200 mm of precipitation annually. The semi-arid climate zone (II)

is primarily located in eastern Mongolia, part of southern Siberia, and most of Inner Mongolia, wherein the annual precipitation is between 200 and 400 mm. The subhumid climate zone (III) accounts for most of the study area, extending across eastern Siberia, northeastern China, and most of the middle and lower reaches of the Yellow River; the annual precipitation in this zone ranges from 400 mm to 800 mm. The humid climate zone (IV) includes all of Japan, the Korean Peninsula, and the middle and lower reaches of the Yangtze River in China; the annual precipitation in this zone is more than 800 mm.

Based on relative indices (Table 2), the NDVI values in the arid climate zone were generally low. The partial correlation coefficients between the seasonal average NDVI and precipitation were high (about 0.55) in the arid climate zone; however, with increasing rainfall, this relationship decreased and exhibited a negative correlation in the humid and subhumid climate zones. The partial correlation coefficients between the seasonal average NDVI and temperature were low, although this relationship was slightly stronger in subhumid areas. The multiple correlation coefficients were also high (about 0.59) in the arid climate zone, and with increasing rainfall, this relationship decreased. Overall, the seasonal average NDVI was highest (about 0.62) in the subhumid climate zone. Thus, the NDVI was identified to be influenced by climatic factors, primarily in the arid and semi-arid climate zones, and was less affected in humid and subhumid climate zones.

To further verify the relationship between the NDVI and climatic factors (e.g., correlations between average trends in seasonal NDVI, precipitation, and temperature in various climate zones), we calculated the relationship between the NDVI, temperature, and precipitation in different climatic regions. Table 3 depicts the results of the regression analyses for the NDVI and climate variables. The stepwise multivariate regression method was used, and two variables were selected to develop the models. The results indicate that the highest adjusted  $R^2$  value was 0.44 for climatic zone (I), whereas the adjusted  $R^2$  values were very low for the other three zones. Based on the coefficients of the two predictor variables, all of the values were low; however, the trend demonstrated that the relationship between the average seasonal NDVI and precipitation was high in the arid climatic zone (I). As the climatic zone gradually became more humid, this correlation weakened. In particular, there was a negative relationship between the average seasonal NDVI and precipitation in the subhumid (III) and humid climate zones (IV). The relationship between the average seasonal NDVI and the temperature was weak in the arid climatic zone (I), but was somewhat stronger in the subhumid climate zone (III). These results are consistent with the previous analysis of partial correlation coefficients.

### An Analysis of Land Cover Changes in Different Climate Zones

In order to better analyze the environmental vegetation changes that occur in this region, we analyzed changes in the land cover classification and land cover conversion that have occurred in the aforementioned climatic zones. Based on AVHRR GLC data that were acquired between 1981 and 1994, and ESA GLC data that were acquired from May 2005 to April 2006, we used a post-classification approach to determine changes in land cover in these two datasets. In Table 4, unchanged areas are located along the major diagonal of the matrix. Conversion values were sorted by area

**Table 3.** Regression Analysis results between NDVI and Climate Variables

Climate zone	Adjusted $R^2$	$F$	Predictors/coefficients	
			Precip.	Temp.
I	0.4440	11.0600	0.0010	0.0060
II	0.0750	2.0600	0.0000	0.0030
III	0.1060	2.5300	-0.0002	0.0130
IV	0.1100	2.6100	-0.0004	0.0100

and listed in descending order. These results indicate that, according to AVHRR and ESA data, grassland areas increased by 3.2% in size, whereas forest areas decreased by 4.9% and cropland areas by 2.0% in size. Regarding land cover conversions, the unchanged area of forest represented 38.0% of the entire area, whereas the conversion area represented a small proportion; however the unchanged grassland and cropland areas covered 9.2% and 7.6% of the entire areas, respectively. The proportions of their conversion areas were large, which may be due to the two different land classification systems that were used. Bare areas, which represented a small proportion of the total study area, increased in size especially rapidly (from 0.3% to 3.7%), which was primarily due to the fact that 3.0% of bare ground was converted from grassland. This expansion will influence the local environment in the future. Additionally, urban areas increased from 0.2% to 0.8%, which represents a small proportion of the entire area, and water areas decreased by 0.3% of the total area, which represents little change.

To further evaluate the results of the land cover conversions, matrices corresponding to land cover changes from the two periods were created for the different climate zones (Table 5). In the arid climate zone (I), the main land cover classifications were grassland and bare ground, wherein 59.8% of the grassland was converted into bare ground, which demonstrates that grassland degradation is a serious problem in this region. In the semi-arid climate zone (II), the total number of pixels that were associated with grassland increased from 11,589 to 13,768, which primarily resulted from the conversion of forest and cropland, representing approximately 2,325 pixels and 3,330 pixels, respectively. The total number of pixels that were associated with forest decreased from 10,528 to 7,937, whereas the total number of cropland pixels decreased from 4,085 to 2,282; however, the amount of bare ground rapidly increased, from 139 pixels to 2,310 pixels, of which 2,084 pixels represented a “grass-to-bare” conversion. In the subhumid climate zone (III), although the forest-associated pixel number decreased from 37,337 to 35,723, forests continued to represent a significant portion of the total investigated land area. Additionally, the area of grassland increased from 7,805 to 11,015 pixels, whereas the area of cropland decreased from 12,875 to 10,415 pixels. Bare ground and urban areas, which were converted from forest, grassland, and cropland, increased from 37 pixels to 579 pixels and from 136 pixels to 605 pixels, respectively. In the humid climate zone (IV), the forest pixel number decreased from 12,143 to 10,427, wherein 2,165 pixels were primarily converted into cropland. Similarly the pixel number that was associated with grassland decreased from 2,093 to 1,998, of which 1,180 were primarily converted into cropland, and as a result, the

**Table 4.** Matrices of Land Cover and Changes from AVHRR to ESA<sup>a</sup>

AVHRR (%)	ESA (%)						AVHRR total
	Forest	Grass	Cropland	Bare	Urban	Water	
Forest	38.0	6.1	4.3	0.2	0.1	0.3	49.0
Grass	1.9	9.2	4.6	3.0	0.3	0.3	19.4
Cropland	3.7	6.9	7.6	0.1	0.3	0.2	18.9
Bare	0.0	0.0	0.0	0.3	0.0	0.0	0.3
Urban	0.0	0.1	0.0	0.0	0.1	0.0	0.2
Water	0.4	0.3	0.3	0.1	0.0	11.2	12.2
ESA total	44.1	22.6	16.9	3.7	0.8	11.9	100.0

<sup>a</sup>AVHRR GLC data acquired between 1981 and 1994; ESA GLC data acquired from May 2005 to April 2006.

amount of cropland increased from 6,193 to 8,035 pixels. Although the amount of bare and urban areas gradually increased, they only represented a small proportion of the total study area.

Overall, although the forest area decreased in size, it still covered 45% of the total study area, and 64% of forest was distributed within the subhumid climate zone. This also explains why the seasonal average NDVI was highest in this region. Additionally, the amount of grassland increased and cropland decreased, primarily in the semi-arid and subhumid climate zones. The amount of bare ground increased in the arid and semi-arid climate zones, primarily because of grassland degradation. The amount of urban area rapidly increased in the subhumid and humid climate zones.

## CONCLUSIONS

This study is intended to enhance the accuracies of the correlations between growth-season NDVI variation, climatic factors, and land cover in northeastern Asia. The multiple linear regression method employed in this study was used to analyze three kinds of satellite data and obtain a standard NDVI variation curve. Although the accuracy of the three-year data (2007, 2008, and 2009) should be verified, the seasonal average results indicate a good degree of adaptation. This method is ideal for large-scale trend variation research.

The significant precipitation boundaries in the investigated region that were associated with different climate zones exhibited a zonal distribution. Based on correlations between the NDVI and the aforementioned climate factors, precipitation is the primary factor that influences the NDVI in the arid climate zone (I), and with increasing precipitation, this influence gradually weakens. The temperature variable was determined not to appreciably affect spatial NDVI changes. We used the annual slope method to analyze NDVI variations. In general, the NDVI values that were averaged for the entire study area exhibited a slightly increasing tendency, and NDVI changes were found to be affected by land cover changes, especially by changes in bare ground, cropland, and grassland.

**Table 5.** Matrices of Land Cover Conversions for Different Climate Zones from AVHRR to ESA

AVHRR (N of pixels)	ESA (N of pixels)						AVHRR total
	Forest	Grass	Cropland	Bare	Urban	Water	
<b>Climate zone (I)</b>							
Forest	6	1	0	1	0	0	8
Grass	0	899	2	1,344	0	1	2,246
Cropland	0	2	0	0	0	0	2
Bare	0	4	0	190	0	2	196
Urban	0	0	0	0	0	0	0
Water	1	1	0	4	0	0	6
ESA total	7	907	2	1,539	0	3	2,458
<b>Climate zone (II)</b>							
Forest	7,662	2,325	487	40	3	11	10,528
Grass	148	8,042	1,209	2,084	32	74	11,589
Cropland	115	3,330	581	40	6	13	4,085
Bare	1	6	0	129	0	3	139
Urban	2	16	0	0	4	0	22
Water	9	49	5	17	0	121	201
ESA total	7,937	13,768	2,282	2,310	45	222	26,564
<b>Climate zone (III)</b>							
Forest	30,087	4,272	2,615	136	71	156	37,337
Grass	1,773	2,108	3,270	279	223	152	7,805
Cropland	3,551	4,483	4,434	109	216	82	12,875
Bare	0	3	0	15	0	19	37
Urban	26	23	9	4	69	5	136
Water	286	126	87	36	26	4,575	5,136
ESA total	35,723	11,015	10,415	579	605	4,989	63,326
<b>Climate zone (IV)</b>							
Forest	8,862	863	2,165	94	14	145	12,143
Grass	465	275	1,180	3	75	95	2,093
Cropland	899	697	4,359	11	133	94	6,193
Bare	0	0	0	0	5	2	7
Urban	7	31	44	1	43	3	129
Water	194	132	287	8	21	8,985	9,627
ESA total	10,427	1,998	8,035	117	291	9,324	30,192

<sup>a</sup>AVHRR GLC data acquired between 1981 and 1994; ESA GLC data acquired from May 2005 to April 2006.

In combination with precipitation, we analyzed land classification changes and land cover conversions in different climatic zones to further analyze the causes of NDVI changes. Based on this analysis, in the arid and semi-arid climate zones (I, II) of northeast Asia, bare areas have gradually expanded, which will influence the region's future environment. Additionally, there is a trend toward a decrease in forests, the primary vegetation type in this region during the 28-year study period. Although the area of grassland has increased, the environmental vegetation changes that have occurred in this region cannot be ignored. Our results suggest that land cover changes and climate change are the factors that influence changes in the NDVI.

In this study, we have created the basis for future research on environmental variations in northeastern Asia. The limitations of this study involve the coarse resolution of the satellite data that were used in the analysis (e.g., the CMAP and CRUTEM3v data). Future research should also incorporate higher spatial resolution data as well as other data types (such as greenhouse gas data) to further evaluate the mechanisms through which these factors interact.

#### ACKNOWLEDGMENTS

We are grateful to all the reviewers for their constructive comments and particularly wish to thank Prof. Jason A. Tullis.

#### REFERENCES

- Anyamba, A. and J. R. Eastman, 1996, "Interannual Variability of NDVI over Africa and its Relation to El Nino/Southern Oscillation," *International Journal of Remote Sensing*, 17:2533–2548.
- Brohan, P., Kennedy, J. J., Harris, I., Tett, S. F. B., and P. D. Jones, 2006, "Uncertainty Estimates in Regional and Global Observed Temperature Changes: A New Dataset from 1850," *Journal of Geophysical Research*, 111:D12106 [doi:10.1029/2005JD006548].
- Chen, X. Q., Tan, Z. J., and M. D. Schwartz, 2000, "Determining the Growing Season of Land Vegetation on the Basis of Plant Phenology and Satellite Data in Northern China," *International Journal of Biometeorology*, 44:97–101.
- Davenport, M. L. and S. E. Nicholson, 1993, "On the Relation Between Rainfall and the Normalized Difference Vegetation Index for Diverse Vegetation Types in East Africa," *International Journal of Remote Sensing*, 14:2369–2389.
- Fensholt, R., Nielsen, T. T., and S. Stisen, 2006, "Evaluation of AVHRR PAL and GIMMS 10-Day Composite NDVI Time Series Products Using SPOT-4 Vegetation Data for the African Continent," *International Journal of Remote Sensing*, 13:2719–2733.
- Fensholt, R., Rasmussen, K., Nielsen, T. T., and C. Mbow, 2009, "Evaluation of Earth Observation Based Long Term Vegetation Trends—Intercomparing NDVI Time Series Trend Analysis Consistency of Sahel from AVHRR GIMMS, Terra MODIS, and SPOT VGT Data," *Remote Sensing of Environment*, 113:1886–1898.
- Gao, Z. and O. Dennis, 2001, "The Temporal and Spatial Relationship between NDVI and Climatological Parameters in Colorado," *Journal of Geographical Sciences*, 4:411–419.

- Gobron, N., Pinty, B., Verstraete, M. M., and J. L. Widlowski, 2000, "Development of Spectral Indices Optimized for the VEGETATION Instrument," In *Proceedings of VEGETATION 2000 Conference*, 3–6 April 2000, Belgirate, Italy, 275–280.
- Goward, S. N., Dye, D. G., Turner, S., and J. Yang, 1993, "Objective Assessment of the NOAA Global Vegetation Index Data Product," *International Journal of Remote Sensing*, 14:3365–3394.
- Gu, Z. H., Chen, J., Shi, P., and M. Xu, 2007, "Correlation Analysis of Normalized Difference Vegetation Index (NDVI) Difference Series and Climate Variables in the Xi Lingole Steppe, China from 1983 to 1999," *Frontiers of Biology in China*, 2:218–228.
- Hansen, M., DeFries, R. J., Townshend, R. G., and R. Sohlberg, 1998, "UMD Global Land Cover Classification, 1 Kilometer, 1.0," Department of Geography, University of Maryland, College Park, MD, 1981–1994.
- Heumann, B. W., Seaquist, J. W., Eklundh, L., and P. Jonsson, 2007, "AVHRR-Derived Phenological Change in the Sahel and Soudan, Africa, 1982–2005," *Remote Sensing of Environment*, 108:385–392.
- Holben, B. N., 1986, "Characteristics of Maximum-Value Composite Images from Temporal AVHRR Data," *International Journal of Remote Sensing*, 7:1417–1434.
- Huete, A., Didan, K., Miura, T., and E. Rodriguez, 2002, "Overview of the Radiometric and Biophysical Performance of the MODIS Vegetation Indices," *Remote Sensing of Environment*, 83:195–213.
- James, M. E. and S. N. V. Kalluri, 1994, "The Pathfinder AVHRR Land Data Set: An Improved Coarse Resolution Data Set for Terrestrial Monitoring," *International Journal of Remote Sensing*, 15:3347–3363.
- Jiang, X. W., Wan, L., Du, Q., and B. X. Hu, 2008, "Estimation of NDVI Images Using Geostatistical Methods," *Earth Science Frontiers*, 15:71–80.
- Kempeneers, P., Lissens, G., and F. Fierens, 2000, "Development of a Cloud, Snow, and Cloud Shadow Mask for VEGETATION Imagery," In *Proceedings of VEGETATION 2000 Conference*, 3–6 April 2000, Belgirate, Italy, pp.303–306.
- Kidwell, K. B., 1990, *Global Vegetation Index User's Guide*, Washington, DC: NOAA/NESDIS, National Climatic Data Center.
- Prince, S. D., 1991, "Satellite Remote Sensing of Primary Production: Comparison of Results for Sahelian Grassland 1981–1988," *International Journal of Remote Sensing*, 12:1301–1312.
- Richard, Y. and I. Poccard, 1998, "A Statistical Study of NDVI Sensitivity to Seasonal and Interannual Rainfall Variations in Southern Africa," *International Journal of Remote Sensing*, 19:2907–2920.
- SPOT Vegetation User's Guide, 2008, [<http://vegetation.cnes.fr/system/content.html#userguide>], accessed September 2008.
- Tarnacsky, E., Garrigues, S., and M. E. Brown, 2008, "Multiscale Geostatistical Analysis of AVHRR, SPOT-VGT and MODIS Global NDVI Products," *Remote Sensing of Environment*, 112:535–549.
- Tieszen, L. L., Reed, B. C., Bliss, N. B., Wylie, B. K., and D. D. DeJong, 1997, "NDVI, C3 and C4 Production, and Distributions in Great Plains Grassland Land Cover Classes," *Ecological Applications*, 7:59–78.

- Townshend, J. R. G., 1994, "Global Data Sets for Land Applications from the Advanced Very High Resolution Radiometer: An Introduction," *International Journal of Remote Sensing*, 15:3319–3332.
- Tucker, C. J., Pinzon, J. E., and M. E. Brown, 2004, *Global Inventory Modeling and Mapping Studies*, College Park, MD: NA94apr15b.n11-VIg, 2.0, Global Land Cover Facility, University of Maryland, College Park.
- Tucker, C. J., Pinzon, J. E., Brown, M. E., Slayback, D. A., Pak, E. W., Mahoney, R., Vermote, E. F., and N. E. Saleous, 2005, "An Extended AVHRR 8-km NDVI Dataset Compatible with MODIS and SPOT Vegetation NDVI Data," *International Journal of Remote Sensing*, 26:4485–4498.
- Tucker, C. J., Slayback, D. A., Pinzon, J. E., Los, S. O., Myneni, R. B., and M. G. Taylor, 2001, "Higher Northern Latitude NDVI and Growing Season Trends from 1982–1999," *International Journal of Biometeorology*, 45:84–190.
- Verbesselt, J., Hyndman, R., Newnham, G., and D. Culvenor, 2010, "Detecting Trend and Seasonal Changes in Satellite Image Time Series," *Remote Sensing of Environment*, 114:106–115.
- Wang, J., Rich, P. M., and K. P. Price, 2003, "Temporal Responses of NDVI to Precipitation and Temperature in the Central Great Plains, USA," *International Journal of Remote Sensing*, 24:2345–2364.
- Wu, S. H., Yang, Q., and D. Zhang, 2003, "Delineation of Eco-geographic Regional System of China," *Journal of Geographical Sciences*, 13:309–315.
- Xie, P. and P. A. Arkin, 1997, "Global Precipitation: A 17-Year Monthly Analysis Based on Gauge Observations, Satellite Estimates, and Numerical Model Outputs," *Bulletin of the American Meteorological Society*, 78:2539–2558.
- Yu, F., Price, K. P., Ellis, J., and P. J. Shi, 2003, "Response of Seasonal Vegetation Development to Climatic Variations in Eastern Central Asia," *Remote Sensing of Environment*, 87:42–54.
- Yuan, F., Sawaya, K. E., Loeffelholz, B. C., and M. E. Bauer, 2005, "Land Cover Classification and Change Analysis of the Twin Cities (Minnesota) Metropolitan Area by Multitemporal Landsat Remote Sensing," *Remote Sensing of Environment*, 98:317–328.